JACS
JOURNAL OF THE AMERICAN CHEMICAL SOCIETY
Article
pubs.acs.org/JACS

# Unfavorable Electrostatic and Steric Interactions in DNA Polymerase β E295K Mutant Interfere with the Enzyme's Pathway

Yunlang Li,[†] Chelsea L. Gridley,[‡] Joachim Jaeger,[‡,§] Joann B. Sweasy,[∥] and Tamar Schlick*[,†]

[†]Department of Chemistry and Courant Institute of Mathematical Sciences, New York University, 251 Mercer Street, New York, New York 10012, United States

[‡]Department of Biomedical Sciences, School of Public Health, University at Albany, 1400 Washington Avenue, Albany, New York 12222, United States

[§]Division of Genetics, Wadsworth Center NYS-DOH, 150 New Scotland Avenue, Albany, New York 12208, United States

[∥]Department of Therapeutic Radiology, Yale University School of Medicine, 333 Cedar Street, P.O. Box 208040, New Haven, Connecticut 06520, United States

Supporting Information

**ABSTRACT:** Mutations in DNA polymerase β (pol β) have been associated with approximately 30% of human tumors. The E295K mutation of pol β has been linked to gastric carcinoma via interference with base excision repair. To interpret the different behavior of E295K as compared to wild-type pol β in atomic and energetic detail, we resolve a binary crystal complex of E295K at 2.5 Å and apply transition path sampling (TPS) to delineate the closing pathway of the E295K pol β mutant. Conformational changes are important components in the enzymatic pathway that lead to and ready the enzyme for the chemical reaction. Our analyses show that the closing pathway of E295K mutant differs from the wild-type pol β in terms of the individual transition states along the pathway, associated energies, and the active site conformation in the final closed form of the mutant. In particular, the closed state of E295K has a more distorted active site than the active site in the wild-type pol β. In addition, the total energy barrier in the conformational closing pathway is 65 ± 11 kJ/mol, much higher than that estimated for both correct (e.g., G:C) and incorrect (e.g., G:A) wild-type pol β systems (42 ± 8 and 45 ± 7 kJ/mol, respectively). In particular, the rotation of Arg258 is the rate-limiting step in the conformational pathway of E295K due to unfavorable electrostatic and steric interactions. The distorted active site in the closed relative to open state and the high energy barrier in the conformational pathway may explain in part why the E295K mutant is observed to be inactive. Interestingly, however, following the closing of the thumb but prior to the rotation of Arg258, the E295K mutant complex has a similar energy level as compared to the wild-type pol β. This suggests that the E295K mutant may associate with DNA with similar affinity, but it may be hampered in continuing the process of chemistry. Supporting experimental data come from the observation that the catalytic activity of wild-type pol β is hampered when E295K is present: this may arise from the competition between E295K and wild-type enzyme for the DNA. These combined results suggest that the low insertion efficiency of E295K mutant as compared to wild-type pol β may be related to a closed form distorted by unfavorable electrostatic and steric interactions between Arg258 and other key residues. The active site is thus less competent for proceeding to the chemical reaction, which may also involve a higher reaction barrier than the wild-type or may not be possible in this mutant. Our analysis also suggests further experiments for other mutants to test the above hypothesis and dissect the roles of steric and electrostatic factors on enzyme behavior.

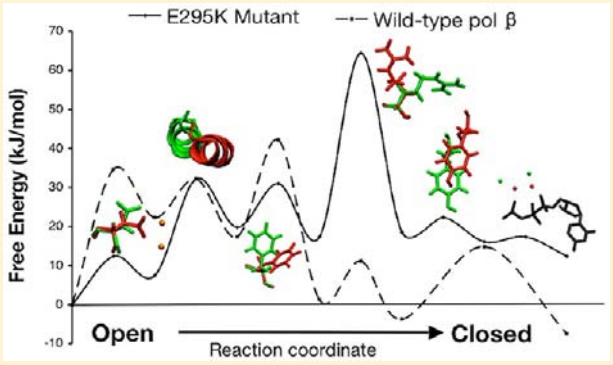


## INTRODUCTION

DNA polymerases are crucial to DNA replication and repair, which are of great importance to maintaining the genomic stability of living organisms. Various cancers, neurological diseases, and premature aging have been related to malfunctions of DNA polymerases.[1−8] The eukaryotic DNA polymerase β (pol β) in the X-family of DNA polymerase functions primarily in base excision repair (BER)[9−11] with moderate accuracy ("fidelity"). In addition, pol β also has 5′-deoxyribose-5-phosphate lyase (dRP lyase) activity[12] during BER. Because BER is considered to play a key role in cancer as well as aging,[13] pol β is important in this context because of its prominent role in BER.[14]

Pol β is shaped like a hand with fingers (Ile88−Pro151), palm (Arg152−Lys262), thumb (Asp263−Glu335) subdomain,

Received: January 12, 2012
Published: May 31, 2012

   dx.doi.org/10.1021/ja300361r | J. Am. Chem. Soc. 2012, 134, 9999−10010

and an 8 kDa domain (Met1−Lys87).[15] X-ray crystallography has provided exquisite views of two forms of the enzyme:[16−18] the closed (ternary, active) and open (binary, inactive) forms are related by a large subdomain motion of the thumb (Supporting Information Figure S1). Kinetic, structural, and computational studies[19−22] have revealed that the catalytic pathway of pol $\beta$ follows the general, three-step nucleotide insertion pathway for DNA polymerases: first, following DNA binding, pol $\beta$ incorporates a 2′-deoxyribonucleoside 5′-triphosphate (dNTP) to form an open complex, which undergoes a conformational change to align active site residues and form a closed complex; second, the closed pol $\beta$ complex catalyzes nucleotidyl transfer reaction and forms the closed product complex; third, the product complex undergoes a reverse conformational change back to the open form, allowing the release of pyrophosphate ($PP_i$). During the conformational steps, besides the large thumb motion, side-chain motions of several key residues such as Asp192, Arg258, Tyr 271, Phe272, and Arg283,[20,22−27] as well as the movements of $Mg^{2+}$ ions,[22,25,28] participate in transitioning the enzyme to/from the reaction competent state. These key residues are also of great importance in controlling pol $\beta$'s fidelity. In mismatched (i.e., not Watson−Crick paired) systems, such key residue motions as well as the related energy barriers are expected to be different.

Depending on the polymerase in question, associated substrates, and other conditions, both conformational and chemical steps can be rate limiting in general.[29] Therefore, an understanding of enzyme catalysis requires knowledge of many steps, conformational and chemical, with the latter being just one part of the big picture.[30] The combined picture of the energy landscape including conformational and chemistry pathways together helps link structural and energetic details with experimental methods and pursue enzyme design applications, for example, to explain the role of different residues, to design mutants with altered functions,[31,32] and to analyze heterogeneous enzyme mixtures where some enzyme becomes trapped in conformational states prior to chemistry.[33−41] The argument that conformational pathways that are not rate limiting overall in the enzyme cycle are not relevant to fidelity[42] is insufficient for analyzing complex kinetic observations and pursuing design applications.

Thirty percent of human tumors studied express DNA pol $\beta$ mutations not present in normal tissue,[4,6,7] including gastric carcinoma-associated pol $\beta$ mutant E295K (glutamic acid to lysine)[5,7] (see Supporting Information Table SI for comparison of kinetic data of pol $\beta$ mutants). The E295K mutant has been shown to be inactive.[5] It interferes with BER and induces sister chromatid exchanges (SCEs) and cellular transformation. However, the dRP lyase activity of the E295K mutant is retained, suggesting that it still can bind to the DNA. Interestingly, not only does the E295K mutant itself lack activity, but it also interferes with wild-type pol $\beta$ during BER when both the mutant and the wild-type pol $\beta$ are present. However, the reason for the inactivity of the E295K mutant and its mode of interference as compared to the wild-type pol $\beta$ remain unclear. It has been hypothesized that the E295K mutant lacks the ability to interact with Arg258 and sequester it away from Asp192.[5]

To help unravel the factors that explain the inactivity of the E295K pol $\beta$ mutant, we use enhanced configurational sampling with the CHARMM all-atom force field (including the cross-term energy correction map specification for proteins[43−45]) to study the closing pathway of E295K before chemistry and compare results to reference systems. Although far from perfect, modeling and simulation have gained accuracy and reliability to study biomolecular systems.[32] Here, we apply transition path sampling (TPS)[46,47] simulations, an approach developed by Chandler and co-workers to traverse high barriers on the free energy surface and capture rare events that are not accessible to regular molecular dynamics (MD) simulations. TPS has been applied to study various systems from small molecules such as peptides and lipids[48−54] to large complex systems.[25,55−59] In a previous work, we have implemented TPS to study the closing and/or chemical pathways of pol $\beta$ complex binding dATP and dCTP, opposite dG[25,55] as well as 8-oxoguanine (8-oxoG).[56] The free energy profiles of those systems emerge as different in terms of both the transition states identified and the associated energy values; these differences, in turn, help interpret differing nucleotide insertion efficiency as revealed experimentally.[20,26,60]

Here, we show that the overall closing energy barrier of the E295K mutant is higher than any of the above four related systems at a significance level of 90% ($65 \pm 11$ kJ/mol versus ($37-45$) $\pm$ 8 kJ/mol).[25,55,56] The rate-limiting step in the conformational pathway before chemistry is the rotation of Arg258, which agrees with the previous hypothesis by Sweasy and co-workers.[5] Our analyses further show that the high energy barrier caused by Arg258 is due to the drastic changes in the electrostatic environment around it, as well as the steric hindrance caused by the Lys295 with Arg258. The distorted active site in the final closed form of the E295K mutant also suggests the hampered activity of the mutant. Interestingly, however, midway through the incorporation of the incoming nucleotide, following the thumb motion but prior to the rotation of Arg258, the E295K mutant has an energy level (within our error bars) similar to that of the wild-type complex; this suggests that the E295K mutant can bind DNA and lock the complex into a partially closed, although inactive, state. This is consistent with the experimental observation that the E295K mutant maintains the affinity for DNA but not the catalytic ability.[5] These differences of E295K from wild-type pol $\beta$ also suggest further experiments on other mutants like E295Y and E295W, where neutral and bulky tyrosine and tryptophan replace Glu295.

## METHODS

**Expression, Purification, and Cocrystallization.** The tagless construct of rat pol $\beta$ was expressed in Rosetta2 DE3 cells as previously described for similar pol $\beta$ constructs.[61] The purification of tagless pol $\beta$ E295K protein is based on a published purification protocol of Klenow Fragment.[62,63] Briefly, the cells were resuspended in 25 mM HEPES, pH 7.0, 100 mM NaCl, 5% glycerol with lysozyme, and the SigmaFAST protease inhibitor cocktail. Cells were sonicated 5 × 30 s for 10 min on ice, followed by centrifugation at 25 700*g*. The protein mixture was syringe filtered through a 5 $\mu$m followed by a 0.45 $\mu$m filter, and then loaded onto a HiTrap Heparin column and separated by a NaCl gradient (buffer A, 25 mM HEPES, 100 mM NaCl, 5% glycerol, pH 7.0; buffer B, 25 mM HEPES, 2 M NaCl, pH 7.0). Fractions containing pol $\beta$ were pooled, diluted 1:5, and purified on a SP Sepharose column (buffer C, 25 mM HEPES, 25 mM NaCl, pH 7.0; buffer B, 25 mM HEPES, 2 M NaCl, pH 7.0). The final purification step consisted of a gel filtration column (HiLoad 16/60 Superdex 75 prep grade, GE Healthcare Bio-Sciences Corp.). Protein was purified and buffer exchanged over the gel filtration column with buffer specific to crystallization of the dsDNA−enzyme complex (0.1 M MES, 10 mM $(NH_4)_2SO_4$, 30 mM NaCl, pH 6.5).

**Table 1. Transition-State Properties for the Closing Conformational Profile of the E295K pol β Mutant**

| TS | event | χ-order parameter | $\chi_{max}$ state A | $\chi_{min}$ state B | $\tau_{mol}$[a] (ps) |
|---|---|---|---|---|---|
| 1 | Asp192 flip | dihedral angle $C_\gamma-C_\beta-C_\alpha-C$ | 150° | 180° | 6 ± 1 |
| 2 | partial thumb motion | rmsd of residues 275−295 with respect to closed form | 3.2 Å | 2.5 Å | 60 ± 10 |
| 3 | Phe272 flip | dihedral angle $C_\alpha-C_\beta-C_\gamma-C_{\delta 2}$ | 110° | 40° | 3 ± 1 |
| 4 | Arg258 rotation, thumb closing | dihedral angle $C_\gamma-C_\delta-N_\varepsilon-C_\zeta$ | 100° | 170° | 12 ± 3 |
| 5 | shift of Tyr271 | distance of Tyr271:OH−Arg283:$N_\varepsilon$ | 6.9 Å | 8.6 Å | 8 ± 1 |
| 6 | ion motion | distance of nucleotide-binding $Mg^{2+}$ to $O_{1\alpha}$ of incoming nucleotide | 4.4 Å | 2.7 Å | 7 ± 1 |

[a]Time required to transverse the transition region as obtained from the correlation function of each transition path sampling (see Supporting Information Figure S3).

Binary complexes of E295K pol β were cocrystallized with DNA in 0.1 M MES, pH 6.5, 30 mM NaCl, and 10 mM $(NH_4)_2SO_4$. For E295K cocrystallization trials, the primer (5′-ATG TGA G-3′) and template DNA (5′-CAA ACT CAC AT-3′) (Integrated DNA Technology) were resuspended in water and annealed 1:1 in 20 mM $MgSO_4$ (90 °C for 2 min, 70 °C for 2 min, 55 °C for 1 min, then cooled to 4 °C by decreasing 0.5 °C every cycle) in a DNA Dyad Peltier Thermal Cycler (MJ Research, Inc.). Protein−DNA mixtures, adjusted to 231 and 289 μM, respectively, were dispensed into 96-well MRC-2 crystallization plates (Hampton Research) for sitting drop crystallization screens and combined 1:1 with reservoir solutions ranging from 120 to 200 mM NaCl, 6−14% PEG3350, 3% glycerol, and 50 mM cacodylate, pH 6.5. Prior to flash-freezing in liquid nitrogen, a cryoprotectant mixture of 15% glycerol plus the mother liquor in the corresponding crystallization well was added to the harvested crystals.

**Structure Determination and Refinement.** X-ray intensity data were collected at 100 K on beamline X4C at the National Synchrotron Light Source in Brookhaven, NY. Data integration and reduction were performed using HKL2000.[64] The structure was determined and phases calculated by molecular replacement (AutoMR/PHASER in PHENIX.1.7.4[65]) followed by rigid body refinement and full atomic refinement with PHENIX interspersed with manual rebuilding in COOT.[66] The final structure was analyzed and verified using COOT, MolProbity,[67] and PyMol.[68]

**System Preparation.** Our starting models are based on the wild-type pol β/DNA substrate complexes from the binary (PDB ID code 1BPX) and ternary (PDB ID code 1BPY) crystal structures,[16] respectively, as well as the binary crystal structure of the E295K mutant (PDB ID code 3V72). Because the binary structure does not contain an incoming nucleotide, a dCTP residue and two binding $Mg^{2+}$ ions are added to pair with the dG template using the ternary crystal structure as reference. The Glu295 in the closed pol β complex is then modified to Lys using the CHARMM program (version c35b2).[69] Manual modifications for Lys295 and nearby residues have been made to reduce possible collisions and provide more possible starting conformations for Lys295, as Lys295 is indicated by the crystal structure to move fast (see results below). Although we have prepared four different pairs of starting models (with different side-chain orientations of several key residues such as Lys295, Arg283, and Phe272, etc.), after the equilibration and targeted MD (TMD) process described below, these structures converge well into one another. Therefore, the starting forms are likely reliable and do not affect our further analysis significantly. All missing atoms are added to the models according to the ternary crystal structure by CHARMM. The $Na^+$ occupying the catalytic ion site in the crystal structure was modified to $Mg^{2+}$ in the binary system.

The system is solvated with the explicit TIP3P water model in a water box via the VMD program.[70] The smallest image distance between the solute and the faces of the periodic cubic cell is set to 7 Å. The total number of water molecules is 12 828. To obtain a neutral system at an ionic strength of 150 mM, 47 $Na^+$ and 27 $Cl^-$ ions are added to the system. All of the $Na^+$ and $Cl^-$ ions are placed at least 8 Å away from both the protein and the DNA atoms and from each other.

The initial model contains 44 918 atoms, 107 crystallographically resolved water molecules from the ternary complex, 12 721 bulk water molecules, two $Mg^{2+}$ ions, incoming nucleotide dCTP, and 47 $Na^+$ and 27 $Cl^-$ counterions.

**Minimization and Equilibration.** Initial energy minimizations and equilibration simulations are performed using CHARMM. The system is minimized with fixed positions for all heavy atoms of protein or nucleotides, using steepest descent (SD) for 10 000 steps followed by the adopted basis Newton−Raphson (ABNR) method for 20 000 steps. The equilibration process is started with a 100 ps simulation at 300 K using the single-time step Langevin dynamics, while keeping all of the heavy atoms of protein or nucleotides fixed. The SHAKE algorithm is then employed to constrain the bonds involving hydrogen atoms. This is followed by unconstrained minimization consisting of 10 000 steps of SD and 20 000 steps of ABNR. The system is then transferred to NAMD[71] and equilibrated for 1 ns at constant pressure and temperature. Pressure is maintained at 1 atm using the Langevin piston method with a piston period of 100 fs, a damping time constant of 50 fs, and a piston temperature of 300 K. The temperature is maintained at 300 K using weakly coupled Langevin dynamics[72] of nonhydrogen atoms with a damping coefficient of 10 $ps^{-1}$. Bonds to all hydrogen atoms are kept rigid using SHAKE, producing good stability with a time step of 2 fs. The system is simulated in periodic boundary conditions with full electrostatics computed using the particle mesh Ewald method[73] with grid spacing on the order of ≤1 Å. Short-range nonbonded terms are evaluated at every step using a 12 Å cutoff for van der Waals interactions and a smooth switching function. The final dimensions of the system are 77.5 Å × 77.3 Å × 77.4 Å.

Following minimization and equilibration, the overall rmsd values (Cα atoms) of the open- and closed-form models relative to their initial structures are 1.14 and 1.26 Å, respectively.

**Temperature Factors.** The temperature factors ($B$ values) are calculated from a regular 10 ns MD simulation of our final model with the expression $B = (8\pi^2/3)\mathrm{MSF}$, where MSF is the mean square fluctuation of each atom.

**Transition Path Sampling Simulations.** The TPS method relies on the idea of importance sampling using standard Monte Carlo (MC) procedures, which explore sequences of states constituting dynamical trajectories[74,75] through random walks. Starting from an initial trajectory (generated here by TMD) that captures a barrier crossing, TPS samples the trajectory space using the Metropolis MC method by performing a random walk with the shooting algorithm;[47] the random walk is biased to make sure that the most important regions of the trajectory space are adequately sampled.[75] The frequency of a trajectory region being visited is determined by its probability so that, even when a random walk is initiated far from a representative transition pathway, the bias can drive the system to important regions of the transition space after sampling. Thus, despite the unphysical nature of the initial sampling trajectory obtained using TMD, the TPS protocol can lead the system to the most important regions and yield physically meaningful trajectories passing through the saddle area. See the Supporting Information for further details on TPS. The most challenging part of TPS is to describe the order parameters representing the transitions. Our prior work was valuable here,[25,55,56] as described next.

To obtain the initial trajectories that connect the two states during the transition, we apply TMD simulations to connect our modeled open and closed forms of the pol β E295K mutant complexes. To choose appropriate order parameters for TPS simulations, we use the

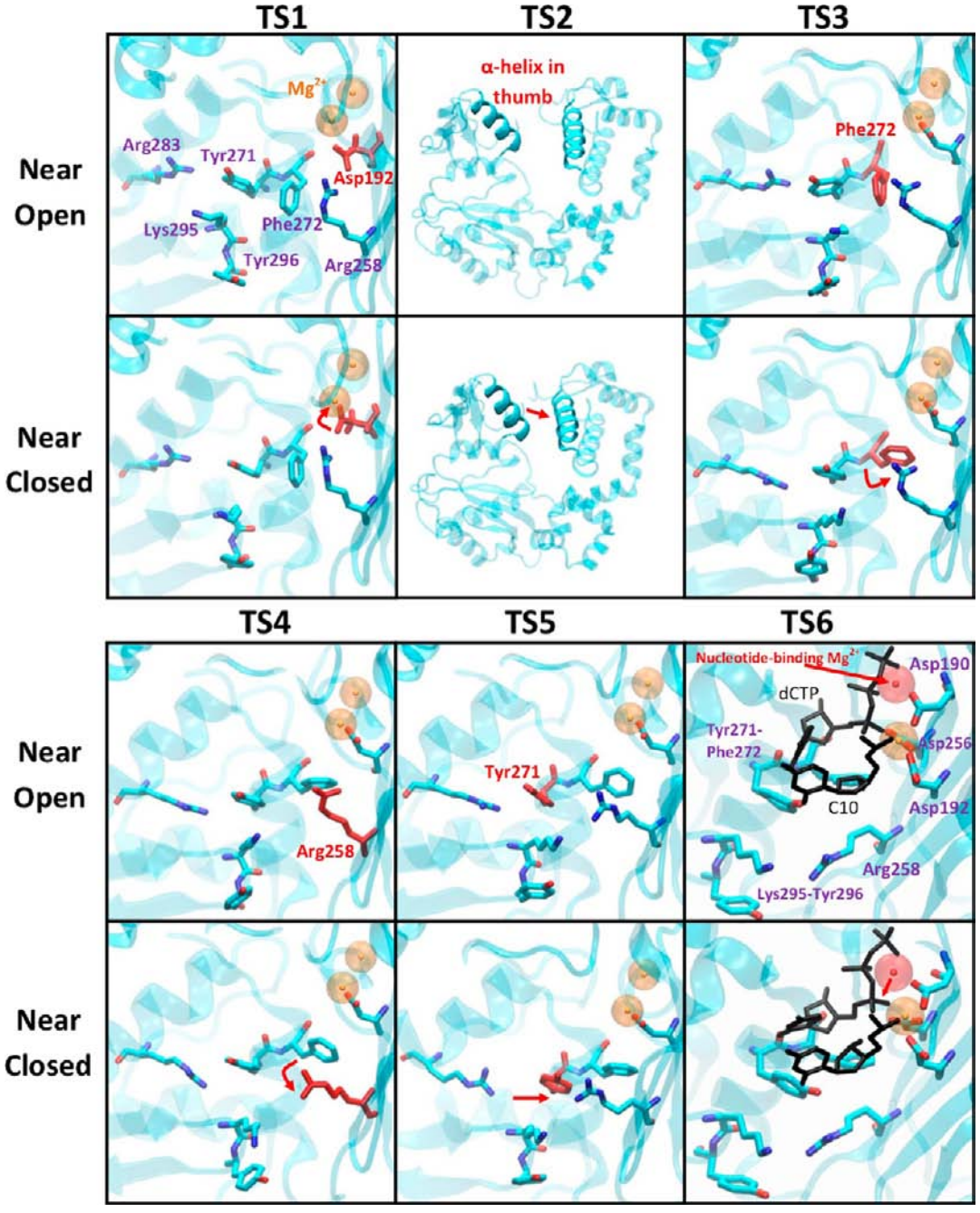


**Figure 1.** Molecular snapshots near open (upper) and closed (lower) states for six transition-state regions. (1) Flip of Asp192. (2) Partial thumb closing. (3) Flip of Phe272. (4) Rotation of Arg258. (5) Shift of Tyr271. (6) Ion rearrangements. $Mg^{2+}$, orange; key residues, purple; dCTP and C10, black; residue characterizing the transition state, red.

crystallographic data,[16] molecular dynamics,[21,22] and prior TPS studies[25,55,56] on wild-type pol $\beta$ as reference. Because these works have shown that key active-site residues (Asp192, Arg258, Tyr 271, and Phe272), the $\alpha$-helix N on the thumb subdomain, and the $Mg^{2+}$ motion serve as measures of pol $\beta$'s closing pathway, we start testing values associated with these residues and ions as well as the rmsd value of $\alpha$-helix N atoms (residues 275−295). When piecing together the entire closing pathway, we found, in addition to above, the complete set of order parameters as listed in Table 1.

We use the TMD code implemented in NAMD to generate the initial constrained trajectories. An energy restraint based on the rms distance of the system relative to the final form is applied to force the open pol $\beta$ complexes to close. The restraint energy can be expressed by:

$$E_{\mathrm{RMS}} = K[D_{\mathrm{RMS}}(X(t), X^{\mathrm{target}}) - d_0]^2$$

In this equation, $K$ is a force constant, $D_{\mathrm{rms}}$ is the relative rms distance for a selected set of atoms between the instantaneous conformation $X(t)$ and the reference $X^{\mathrm{target}}$, and $d_0$ is an offset constant (in Å). In our TMD simulations, the rms distance is evaluated using the heavy atoms on the pol $\beta$ mutant. A total force constant of 3000 kcal $mol^{-1}$ $Å^{-2}$ is applied to all heavy atoms of the complex. The offset parameter $d_0$ is set to decrease from 5.2 Å to 0 in 400 ps, as the mutant is driven from the open to the closed form. From the TMD trajectory, six transition regions are identified (Table 1 and Supporting Information Figure S2).

From the TMD trajectory, we select frames that bracket the transition regions associated with specific residues/ions and thumb conformational changes and perform unconstrained dynamics simulations. We perturb the atomic momenta of the frames and


dx.doi.org/10.1021/ja300361r | J. Am. Chem. Soc. 2012, 134, 9999−10010

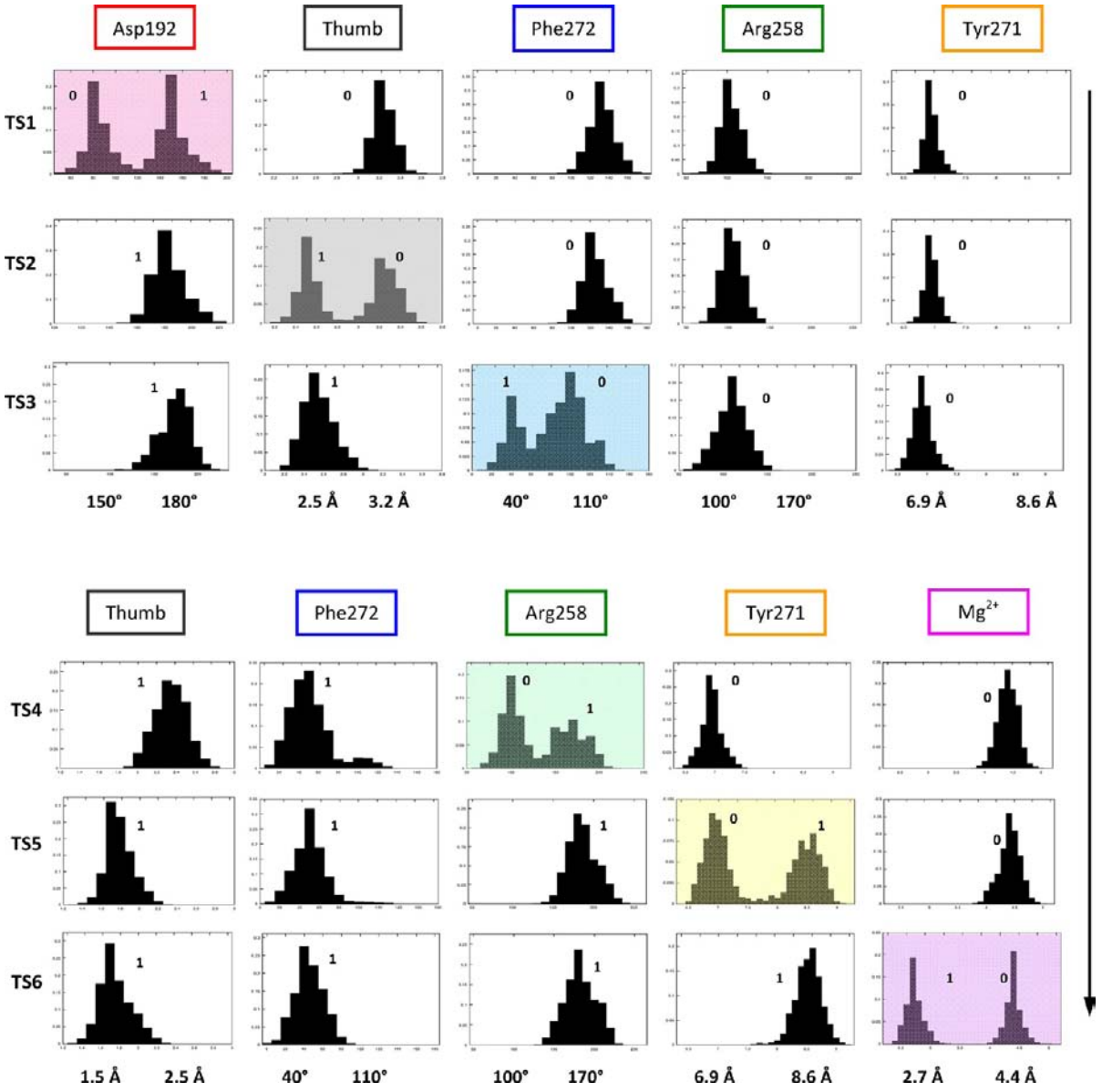


**Figure 2.** Normalized probability distribution of the order parameters for the transition states revealed (TS1−TS6). Labels 0 and 1 indicate the open- and closed-form conformations.

integrate the equations of motion forward and backward over short trajectories of order 10−100 ps (see below) to generate new physical, unbiased trajectories that connect the open and closed states of pol $\beta$. On the basis of these unconstrained simulations, we determine the adequate length of sampling trajectories for all of the transition states. Specifically, for the mutant complex, the trajectories for Arg258 rotation are simulated for 20 ps, and those trajectories for other key residue and $Mg^{2+}$ motions are run for 10 ps. To capture the transition states of thumb closing in the two complexes, the sampling trajectories have to be propagated for 100 ps.

Using one of the newly generated physical trajectories as the starting trajectory, we perform path sampling for each individual conformational change with the shooting and shifting algorithm and a Monte Carlo protocol. The entire process is performed by using a PERL script that interfaces with NAMD to generate new trajectories. The velocity Verlet integrator in NAMD with a time step of 1 fs is used for generating the individual molecular dynamics trajectories in TPS. All other parameters are the same as those in the equilibration process. To obtain an acceptance rate of 30−45%, the momentum perturbation magnitude (d$P$) of each transition state is varied from 0.001 to 0.005. A total of 200 accepted trajectories is collected to map each transition state.

The convergence of the harvested sampling trajectories is verified by computing the autocorrelation function associated with order parameters to check for decorrelation of paths (see the Supporting Information and Figure S3). The new trajectories are essentially decorrelated if the autocorrelation function shows a gradual transition between $\langle\chi_A\rangle^2$ and $\langle\chi_A\rangle\langle\chi_B\rangle$.

**Free Energy Barrier and Rate Constant Calculations.** The free energy barriers for transition states are evaluated using the "BOLAS" protocol,[76] an efficient procedure for getting free energies with relatively low error bars using the TPS trajectory harvesting idea. We divide the reaction coordinate of each transition into 10 small overlapping windows and perform umbrella sampling to generate 500 trajectories on each window. We then combine the potential of mean force plots obtained from the sampling calculations on each window by adding/subtracting a constant to match the free energy values of the overlapping region. From the overall free energy plots, we calculate the free energy barriers for the conformational transitions. The error bar for the free energy calculations is determined by repeating umbrella sampling on one window of a transition five times with the


dx.doi.org/10.1021/ja300361r | J. Am. Chem. Soc. 2012, 134, 9999−10010

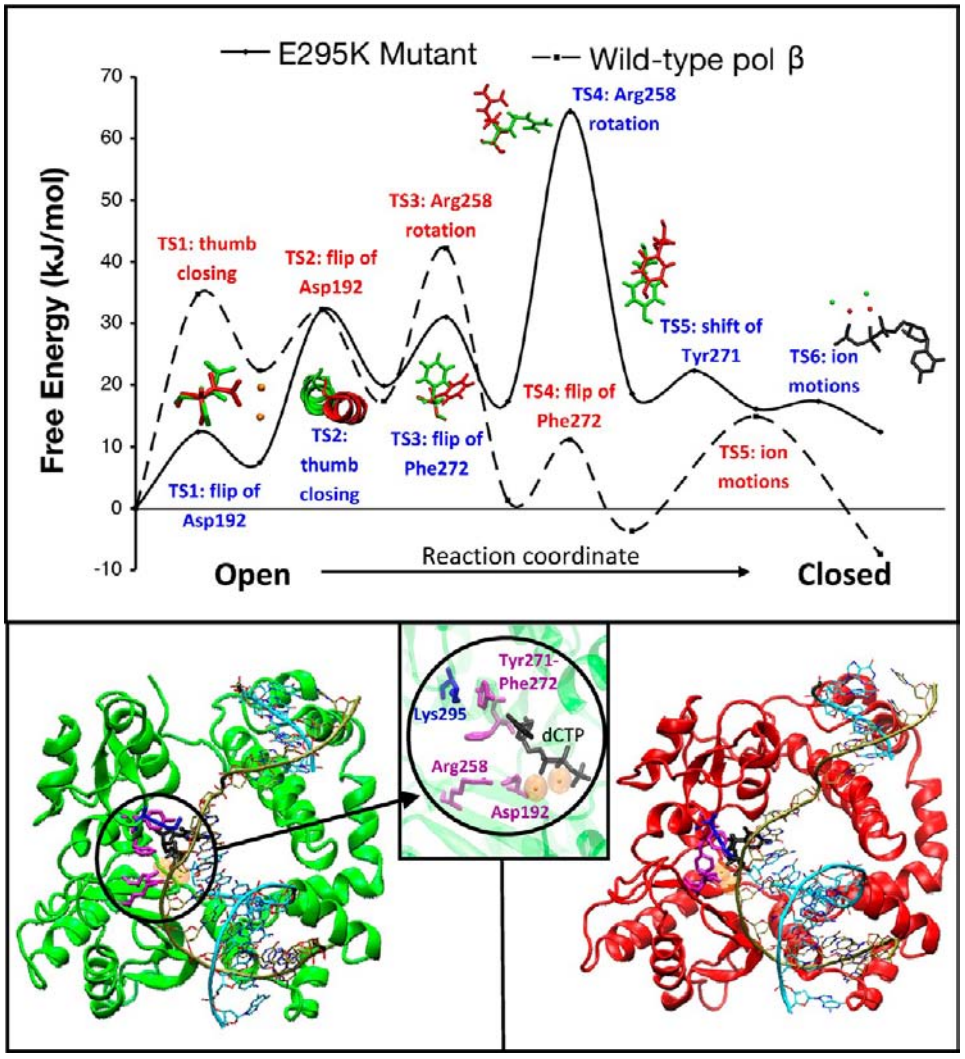


**Figure 3.** The free energy profile of the pol $\beta$ E295K mutant system. The superimposed dashed line is the free energy profile of the wild-type pol $\beta$ system. The open and closed forms of the E295K mutant are drawn in green and red, respectively. $Mg^{2+}$, orange (except in the diagram of ion motions, where green and red are used); dCTP, black; Lys295, blue; key residues involved in transition states (Asp192, Arg258, Tyr271, and Phe272), purple.

same initial trajectory but different starting pseudorandom numbers. The standard deviation for each barrier (3–6 kJ/mol) is used as the error bar and is comparable to prior works.[25,55,56]

The rate of the transition between adjoining metastable states is estimated using transition-state theory as:

$$k_{\mathrm{TST}}^{\mathrm{AB}} = \frac{1}{\tau_{\mathrm{mol}}} e^{-\beta \Delta F_{\mathrm{AB}}^{\mathrm{barrier}}}$$

where the characteristic relaxation time $\tau_{\mathrm{mol}}$ is estimated by the time taken from the gradual transition of the autocorrelation function $\langle \chi_i(0)\chi_i(0)\rangle$.

## RESULTS

**Crystallographic Studies.** The crystals of the pol $\beta$ E295K binary complex belong to space group $P2_12_12_1$ with one molecule per asymmetric unit (cell dimensions of $a$ = 57.2 Å, $b$ = 73.8 Å, $c$ = 118.4 Å and $\alpha,\beta,\gamma$ = 90.0°, $V_m$ = 2.66 Å$^3$/Da). The crystal structure (PDB ID code: 3V7L) was refined using data extending to 2.49 Å Bragg spacings, and the final model shows excellent agreement with the density maps throughout ($R$-free = 0.29, root mean square (rms) deviations bonds = 0.009 Å, and angles = 1.13°). A representative region of the density map near the site of mutation is shown in Supporting Information Figure S4, with the map contoured at 1.25 rms above the mean electron density in the asymmetric unit. The DNA template strand and adjacent residues Arg258, Tyr271, Phe272, Arg283, and Tyr296 are very well-defined. The residues adopt the same position seen in related binary complexes of wild-type pol $\beta$ (1BPY). However, the lack of electron density for Lys295 (atoms C$\beta$ to N$\zeta$) is striking and indicative of fast moving, ill-defined side-chain atoms. The lack of definition in the electron density corresponding to the Lys295 side-chain atoms is in excellent agreement with the flexibility of this residue observed during the simulations. The temperature factors of the Lys295 side-chain atoms are up to 1.5 times higher than those of the immediately adjacent tyrosine residues (Tyr271 and Tyr296). The experimental temperature factors agree well with those obtained from MD simulations (Supporting Information Figure 5).

**Transition-State Identification.** Our analyses of detailed closing pathways before chemistry identify six transition states (Figure 1), as compared to five and four transition states for matched (correct Watson–Crick base pair between the


dx.doi.org/10.1021/ja300361r | J. Am. Chem. Soc. 2012, 134, 9999–10010

**Table 2. Free Energy Barrier and Rate $k_{TST}$ Estimated by Transition-State Theory**

| | Asp192 flip | thumb closing | Phe272 flip | Arg258 rotation | Tyr271 shift | ion motions | total[a] |
|---|---|---|---|---|---|---|---|
| | | | | E295K Mutant | | | |
| $\beta\Delta F_{AB}^{barrier}$[b] | 12 ± 4 | 25 ± 5 | 12 ± 4 | 47 ± 6 | 4 ± 3 | 2 ± 3 | 65 ± 11 |
| $\beta\Delta F_{BA}^{barrier}$ | 6 ± 3 | 12 ± 3 | 14 ± 4 | 46 ± 6 | 6 ± 3 | 5 ± 3 | 51 ± 7 |
| $k_{TST}^{A\to B}$ ($s^{-1}$) | $1.1 \times 10^9$ | $7.6 \times 10^5$ | $3.7 \times 10^9$ | $4.7 \times 10^2$ | $2.8 \times 10^{10}$ | $8.6 \times 10^{10}$ | |
| $k_{TST}^{B\to A}$ ($s^{-1}$) | $2.2 \times 10^{10}$ | $1.2 \times 10^8$ | $1.4 \times 10^9$ | $7.7 \times 10^2$ | $1 \times 10^{10}$ | $1.9 \times 10^{10}$ | |
| | | | | Wild-type: Matched System (G:C) | | | |
| $\beta\Delta F_{AB}^{barrier}$ | 10 ± 4 | 35 ± 5 | 10 ± 3 | 25 ± 4 | | 19 ± 5 | 42 ± 8 |
| $\beta\Delta F_{BA}^{barrier}$ | 15 ± 4 | 12 ± 3 | 15 ± 4 | 40 ± 6 | | 22 ± 4 | 49 ± 8 |
| $k_{TST}^{A\to B}$ ($s^{-1}$) | $(5 \times 10^9)^c$ | $(1.2 \times 10^4)^c$ | $(5 \times 10^9)^c$ | $(2.5 \times 10^7)^c$ | | $2 \times 10^9$ | |
| $k_{TST}^{B\to A}$ ($s^{-1}$) | $(6 \times 10^8)^c$ | $(1 \times 10^8)^c$ | $(6 \times 10^8)^c$ | $(1 \times 10^4)^c$ | | $3 \times 10^7$ | |
| | | | | Wild-type: Mismatched System (G:A) | | | |
| $\beta\Delta F_{AB}^{barrier}$ | 15 ± 3 | 36 ± 5 | 15 ± 4 | 2 ± 2 | | | 45 ± 7 |
| $\beta\Delta F_{BA}^{barrier}$ | 15 ± 4 | 6 ± 4 | 20 ± 5 | 5 ± 3 | | | 23 ± 6 |
| $k_{TST}^{A\to B}$ ($s^{-1}$) | $(6 \times 10^8)^c$ | $(6 \times 10^3)^c$ | $6 \times 10^8$ | | | | |
| $k_{TST}^{B\to A}$ ($s^{-1}$) | $(6 \times 10^8)^c$ | $(1 \times 10^9)^c$ | $2 \times 10^7$ | | | | |

[a]The total energy barrier for conformational pathway before chemistry from open to closed state. [b]$\Delta F_{AB}^{barrier}$ is the free energy of the transition-state region between basins A and B relative to basin A, in kJ/mol. Detailed free energy plots for each transition are shown in Figure S6. [c]To make the energy values comparable, the orders of events in the table for systems other than E295K have been rearranged as reflected by values in parentheses. See Supporting Information Table SII for the sequence of transition states in each system.

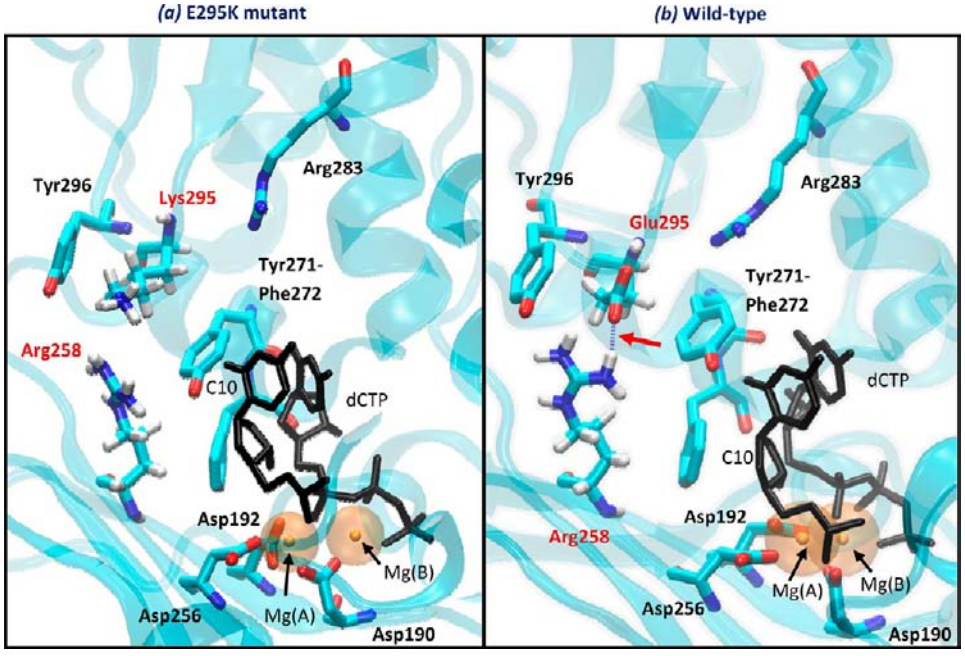


**Figure 4.** Representative active site conformation of (a) E295K mutant and (b) wild-type pol $\beta$ in the final closed form. Dashed lines indicate hydrogen bonds. Mg(A), catalytic ion; Mg(B), nucleotide-binding ion; C10, the base in the upstream primer DNA strand, which will connect with dCTP during the chemical step.

incoming nucleotide and the template base, G:C)[25] and mismatched (incorrect Watson–Crick base pair, G:A)[55] wild-type systems, respectively. The sequence of changes along the pathway of the E295K mutant is illustrated in Figure 1: (1) flip of Asp192; (2) partial thumb closing; (3) flip of Phe272; (4) rotation of Arg258; (5) shift of Tyr271; and (6) ion rearrangement characterized by the shift of nucleotide-binding $Mg^{2+}$ (Table 1). Each transition state is characterized by the probability distribution in Figure 2. The existence of two peaks (marked by 0 and 1) within one plot implies a conformational transition across the energy barrier. Therefore, a path sampling trajectory of TS1–TS6 captures the entire conformational pathway.

The first transition captured in our mutant system is the flip of Asp192, while in wild-type pol $\beta$ systems, the flip of Asp192 almost always happens after the partial thumb closing, except in the 8-oxoG:C system, which lacks this transition state. Furthermore, following partial thumb closing, the next residue to rearrange in E295K is Phe272; this sequence occurs in the G:A mismatched system but not in the other wild-type systems, where the rotation of Arg258 occurs not after, but before, Phe272. The thumb remains half-closed (rmsd of residues 275–295 relative to the closed structure is ~2.5 Å) until the flip of Phe272 and rotation of Arg258 are completed (final rmsd is ~1.6 Å). The shift of Tyr271 was not characterized as a transition state in our previous TPS studies on wild-type pol $\beta$ systems, although a similar shift of Tyr271 was captured using


dx.doi.org/10.1021/ja300361r | J. Am. Chem. Soc. 2012, 134, 9999–10010

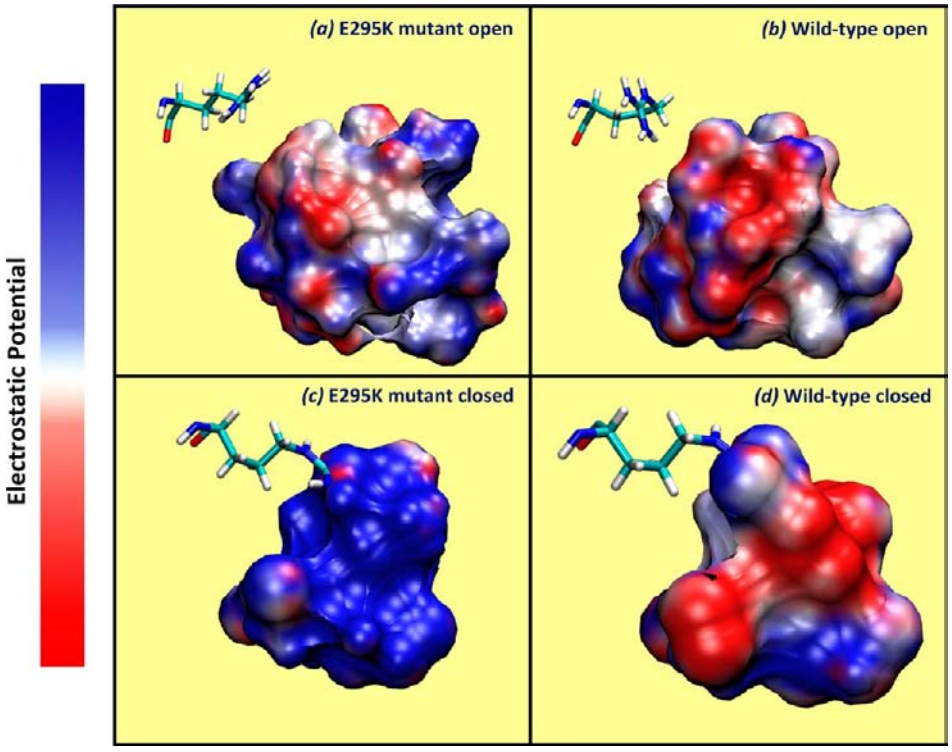


**Figure 5.** Electrostatic potential landscapes of residues around Arg258 in (a) E295K mutant open form, (b) wild-type pol $\beta$ open form, (c) E295K mutant closed form, and (d) wild-type pol $\beta$ closed form. Residues within 4 Å of Lys295/Glu295 are shown in the figure, including Cys267, Gly268, Tyr271, Arg283, Asn294, Lys295, Tyr296, and Thr297.

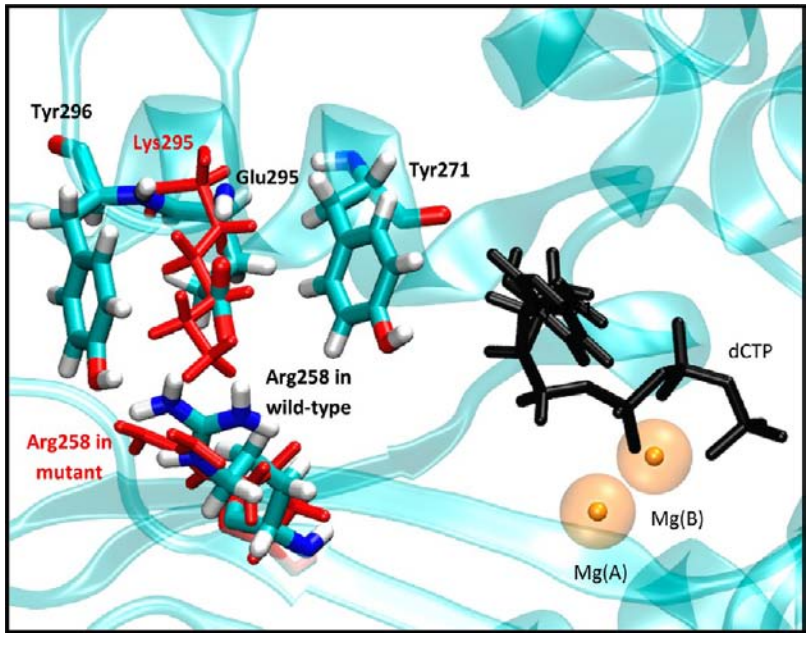


**Figure 6.** "Sandwich-shaped" structure formed by Glu295/Lys295, Tyr296, and Tyr271 tends to cause steric hindrance for Arg258 in the E295K mutant complex. The residues Lys295 and Arg258 (red) from the final closed form of the E295K mutant are superimposed onto the ternary crystal structure of wild-type pol $\beta$. Mg(A), catalytic ion; Mg(B), nucleotide-binding ion.

the stochastic difference equation (SDEL) method.[22] Here, we observe that Tyr271 shifts after all other key residue motions are completed, which agrees with our previous observation that Tyr271 only moves after the transition state is stabilized by the thumb closing and the active site assembly.[22] Following the motions of the thumb and key residues, subtle ion motions occur to seal rearrangements of the active site prior to the chemical reaction step.

**Potential of Mean Force Calculation.** The free energy changes associated with each transition event are used to construct the overall reaction kinetics profiles in Figure 3 (also see Supporting Information Figure S6). The barriers corresponding to TS5 (shift of Tyr271) and TS6 (ion rearrange-


dx.doi.org/10.1021/ja300361r | J. Am. Chem. Soc. 2012, 134, 9999−10010

**Table 3. Average Critical Distances for the Chemical Reaction Following the Final Transitions of pol β/DNA Complexes in Different Systems**

| critical distance (nm) | E295K mutant (G:C) | wild-type (G:C) | wild-type (G:A) | wild-type (8-oxoG:C) | wild-type (8-oxoG:A) |
|---|---|---|---|---|---|
| Mg(A)[a]−O1α | 1.8 ± 0.2 | 1.8 ± 0.2 | 3.8 ± 0.2 | 6.4 ± 0.5 | 4.4 ± 0.3 |
| Mg(A)−O3′ | 5.6 ± 0.3 | 4.2 ± 0.3 | 5.9 ± 0.4 | 2.0 ± 0.2 | 7.0 ± 0.4 |
| Mg(A)−OD1−Asp192 | 1.8 ± 0.2 | 1.8 ± 0.1 | 1.8 ± 0.1 | 1.8 ± 0.2 | 1.9 ± 0.2 |
| Mg(A)−OD2−Asp256 | 1.7 ± 0.2 | 1.8 ± 0.2 | 1.8 ± 0.2 | 1.8 ± 0.3 | 1.8 ± 0.1 |
| Mg(B)−O1α | 2.7 ± 0.2 | 1.9 ± 0.3 | 1.8 ± 0.2 | 1.9 ± 0.2 | 1.9 ± 0.3 |
| O3′−Pα | 4.8 ± 0.3 | 4.1 ± 0.2 | 5.3 ± 0.3 | 6.7 ± 0.4 | 5.5 ± 0.4 |

[a]Mg(A) represents the catalytic $Mg^{2+}$; Mg(B) represents the nucleotide-binding $Mg^{2+}$; O1α represents O1α on the dNTP; O3′ represents O3′ on the Cyt10 in the upstream primer DNA strand, which will be connected to the dNTP in the chemical step; Pα represents Pα on the dNTP.

ments) are small as compared to TS1−TS4: given the value ∼5 ± 3 kJ/mol, they may be negligible overall. The overall activation free energy for the conformational pathway in the mutant system is notably higher than that of the wild-type system at a 90% significance level: 65 ± 11 kJ/mol versus 42 ± 8 kJ/mol. The higher conformational energy barrier may hamper the system to reach the active closed form. On the basis of these free energy values, we compute the rate constants for each transition in Table 2.

The high energy barrier of the E295K mutant mainly arises from the large barrier of Arg258, which is 47 ± 6 kJ/mol, much higher than the 25 ± 5 kJ/mol barrier of Arg258 rotation in the wild-type system at a 95% significance level. In Figure 4, we compare the key residues around the active site in both the E295K mutant and the wild-type system. Significantly, the hydrogen bond between Arg258 and Glu295 in the wild-type system, which may help stabilize the position of Arg258 in the closed form, is missing in the mutant system. Experiments show that this hydrogen bond is also crucial for promoting the binding of the catalytic ion in the final closed state.[77] Besides the lack of this hydrogen bond, as shown in Figure 5, the electrostatic surface of the E295K mutant in both the open and the closed forms is generally positive, while the surface of the wild-type system is more negative. This difference is mostly due to the difference of charge between Lys295 and Glu295, as well as the electronic effect, field effect, of Lys295/Glu295 on nearby polarizable residues such as Tyr271 and Tyr296. The effect of electrostatic repulsion is also reflected in the difference of final distances between Arg258 and Lys295/Glu295 (5.4 and 4.2 Å, R258:CZ−K295:NZ and R258:CZ−E295:CD, respectively), which shows that Arg258 is distorted in the mutant. Thus, the rotation of Arg258 in the mutant is unfavorable due to electrostatic repulsion.

We superimpose the final structures of both wild-type and mutant systems in Figure 6. The Lys295/Glu295 is buried between two tyrosines (Tyr296 and Tyr271), forming a sandwich-shaped structure. This "sandwich-shaped" structure is quite stable during our simulations, and it is also notable in the crystal structure of the E295K mutant (Figure S4). Therefore, although Lys295 appears to be flexible during our simulation, the position that Lys295 may adapt is constrained in a limited space between those two tyrosines. Because of the longer length of the side chain of Lys295 as compared to Glu295, Arg258 has to adapt a further distorted conformation in the closed form of the mutant to keep a longer distance from Lys295. Even with a hydrogen-bond acceptor for Arg258, Arg258 has to be distorted to form the hydrogen bond because of steric hindrance. As a result, the rotation of Arg258 is difficult to complete in the E295K mutant system due to both the electrostatic repulsion and the steric clash. This finding also agrees with the experimental observation that the E295A mutant can still complete its catalytic pathway although it has reduced activity[78] (see Supporting Information Table SI and Figure S7). Because alanine is neutral and less bulky than lysine, both electrostatic repulsion and steric clash in the E295A system would be reduced, and therefore the rotation of Arg258 would be more facile to accomplish as compared to that in the E295K system.

## DISCUSSION

We have described the conformational closing profiles of the pol β E295K mutant by TPS simulations. Important differences in the conformational profiles between the mutant and wild-type systems are observed concerning distortion of the closed versus open state, the various transition states, and their order, overall energy barrier, and electrostatic and steric factors.

First, the active site conformation in the final closed state of E295K is distorted (Table 3). The active site of the mutant E295K deviates from that of the wild-type G:C with regard to O3′−Pα, catalytic $Mg^{2+}$−O3′, and nucleotide-binding $Mg^{2+}$−O1α distances. Notably, the distance between the nucleotide-binding $Mg^{2+}$ and O1α in the mutant system is significantly longer than that distance in all four wild-type systems (G:C, G:A, 8-oxoG:C, and 8-oxoG:A) at a 95% significance level. Therefore, the closed form of the mutant is more distorted than that of the wild-type. Following the transition of the active site conformation, the crucial metal ion distances in the mutant system are far from the ideal values required for the nucleotidyl-transfer reaction; thus, the mutant system must undergo more significant rearrangements prior to the chemical reaction to assemble the metal ions in the proper positions, and these likely involve additional energy barriers.[21,22,79] In comparison to the G:A mismatched and 8-oxoG pol β closed state, E295K is overall less distorted than both G:A (in terms of the shift of Arg283, $Mg^{2+}$ ions, and O3′−Pα distance,[55,79] at a 95% significance level) and 8-oxoG systems, which may have additional stabilizing features. However, the mutant must undergo a larger barrier to reach that state (see below).

Second, the flip of Asp192 occurs very early in the E295K mutant system. However, after the flip of Asp192, the free energy of the system increases by 6 kJ/mol, while in the wild-type G:C, G:A, and 8-oxoG:C systems, the free energy decreases by 0−5 kJ/mol (in the 8-oxoG:A system, the flip of Asp192 is not a step in the pathway). In the open form, Arg258 forms a hydrogen bond with Asp192, which attracts Asp192 and stabilizes the position of Asp192 before it flips to $Mg^{2+}$. In the E295K mutant, the positively charged Lys residue replaces the negatively charged Glu. Therefore, the electrostatic environment along the side of Arg258 becomes more positive, attracting Asp192 more. As a result, Asp192 tends more to


dx.doi.org/10.1021/ja300361r | J. Am. Chem. Soc. 2012, 134, 9999−10010

revert back (away from $Mg^{2+}$) in the mutant system, and thus the system following the Asp192 flip becomes less favored. In other words, unlike the wild-type systems, the flip of Asp192 in the E295K mutant does not make the remaining energy pathway "downhill".

Third, the overall energy barrier for the partial closing of the thumb, roughly the first half of the conformation pathway, is 31 kJ/mol in the mutant system, similar to that of 35 kJ/mol in the wild-type matched system and 36 kJ/mol in the wild-type mismatched system. Furthermore, the partially closed form before the Arg258 rotation has a similar energy level (within our error bars) as compared to those of the wild-type systems (17 and 18−25 kJ/mol, respectively). Therefore, the E295K mutant may compete with the wild-type enzyme. However, because of the high energy barrier in the following steps, the partially closed form of the E295K mutant may be less likely to continue its conformational pathway. In fact, our 100 ns regular MD simulation of the mutant from the open form indicates that the mutant can easily transit into the partially closed form after the thumb closing and remain in that form, without further key residue motions such as the rotation of Arg258. This finding agrees with the experimental observations that not only is the E295K mutant itself inactive, but it also interferes with the ability of wild-type pol $\beta$ to catalyze DNA synthesis on single nucleotide gaps.[5] E295K binds to single-nucleotide gapped DNA with an affinity that is similar to that of wild-type pol $\beta$, but could bind to the 3′OH of the gap and block access to wild-type pol $\beta$. Alternatively, the partially closed form of E295K may compete with the similar structure of wild-type pol $\beta$. Importantly, E295K has dRp lyase activity that is similar to that of wild-type pol $\beta$, suggesting that stabilization of the closed form of pol $\beta$ is not necessary for this activity. Thus, the lyase reaction could involve a more open or completely open conformation of pol $\beta$ and occur before closure or after the opening of the protein, following chemistry.

Last but not least, the main difference in the conformation pathway of the mutant compared to wild-type systems lies in Arg258. We have shown that both the electrostatic effect and the steric hindrance affect the rotation of Arg258; yet, which effect is more significant still remains unclear. We suggest that mutations such as E295Y and E295W may help delineate this question. If steric hindrance is more important, mutations like tyrosine and tryptophan with neutral but bulky side chains should also inactivate the polymerase; if the electrostatic effect is more important, such mutations may deteriorate the catalytic ability of pol $\beta$ but not inactivate it completely.

Kinetic data show that the overall catalytic process (both conformational and chemical changes) for the matched wild-type pol $\beta$ system has an energy barrier of 65−70 kJ/mol (calculated from experimental data of the intrinsic rate constant of polymerization $k_{pol}$[19,20,26,60,78,80−87]), which is similar to the conformational barrier for the mutant we obtain here, and chemistry is believed to be rate-limiting overall (Figure S6). In the E295K mutant, the conformational pathway, especially the rotation of Arg258, already hampers significantly the enzyme's ability to reach a chemical-reaction competent state. As observed in other DNA polymerases, an altered enzyme complex may also have a different rate-limiting step (chemical or conformational) from the wild-type system. For example, for *Sulfolobus solfataricus* P2 DNA polymerase IV, the rate-limiting step is the chemical step for the matched (correct base) system, but the conformational step is rate-limiting for the mismatched system (incorrect base).[88] For pol I from bacteria *Bacillus stearothermophilus*, the energy barrier for the chemical step is higher than that for the conformational changes (64 versus 61 kJ/mol)[89] with a normal G:C base-pair; with a 8-oxoG:C base-pair, the energy barrier for the chemical step drops to 29 kJ/mol.[90] For the E295K pol $\beta$ mutant, in vitro work indicates no incorporation of dNTP even in excess amounts of substrate (Sweasy, unpublished work); thus, this mutant may not be able to go through the chemical step. Additional studies are needed for a final determination.

## CONCLUSION

Our binary E295K complex together with computational investigation of the E295K pol $\beta$ mutant using the transition path sampling simulations reveal the conformational transition pathway before chemistry for this mutant. As compared to previous work on several wild-type systems,[25,55,56] the conformational pathway of the mutant is different regarding both the sequence of events and the individual energy values. Six transition regions are identified, and these provide a combined energy barrier of 65 ± 11 kJ/mol. The active site in the final closed form of the mutant is distorted. The rate-limiting step in the conformational pathway is the rotation of Arg258. The rotation is hampered due to both steric and electrostatic effects. Furthermore, the mutant's partially closed form, which forms after the partial thumb closing but before the key residue motions of Arg258 of the E295K mutant, has a similar energy level as compared to that of the wild-type pol $\beta$ within the computed error bars. This suggests the possibility that the mutant may bind with DNA and undergo thumb closing as easily as the wild-type, but due to the high energy barriers in the following steps it may be difficult for the mutant to continue on its pathway. Therefore, when both the mutant and the wild-type pol $\beta$ are present, the E295K mutant competes with wild-type pol $\beta$, and the activity of the wild-type could deteriorate. Because kinetic data suggest the inactivity of E295K, chemistry may be associated with a very high energy barrier. Further experimental kinetic and crystallographic work as well as modeling work using quantum mechanics/molecular mechanics (QM/MM) calculations are needed to relate the conformational and chemical barriers for the mutant.

## ASSOCIATED CONTENT

### Supporting Information

Shooting algorithm and test of convergence of TPS, Supplemental Tables SI−SIII, and Figures S1−S9. This material is available free of charge via the Internet at http://pubs.acs.org.

## AUTHOR INFORMATION

### Corresponding Author

schlick@nyu.edu

### Notes

The authors declare no competing financial interest.

## ACKNOWLEDGMENTS

We thank Dr. Ravi Radhakrishnan for providing the initial scripts for transition path sampling simulations. Research described in this Article was supported in part by Philip Morris USA Inc. and Philip Morris International and by NSF award MCB-0316771, NIH award R01 ES012692, and the American Chemical Society's Petroleum Research Fund award (PRF #39115-AC4) to T.S., and NCI award 2R01CA08030 to J.J. and

J.B.S. Access to beamline NSLS-X4C at the New York Structural Biology Center and the core facilities at the Wadsworth Center is gratefully acknowledged. The computations were conducted using the resources of the CCNI supported by the New York State Foundation for Science, Technology and Innovation (NYSTAR), and the Dell computer cluster by New York University Information Technology Services (NYU ITS). Molecular images were generated using the VMD[70] and PyMol[68] programs.

## REFERENCES

(1) Jackson, S. P.; Bartek, J. *Nature* **2009**, *461*, 1071.
(2) Hoeijmakers, J. H. *N. Engl. J. Med.* **2009**, *361*, 1475.
(3) An, C. L.; Chen, D. S.; Makridakis, N. M. *Hum. Mutat.* **2011**, *32*, 415.
(4) Dalal, S.; Chikova, A.; Jaeger, J.; Sweasy, J. B. *Nucleic Acids Res.* **2008**, *36*, 411.
(5) Lang, T. M.; Dalal, S.; Chikova, A.; DiMaio, D.; Sweasy, J. B. *Mol. Cell. Biol.* **2007**, *27*, 5587.
(6) Starcevic, D.; Dalal, S.; Sweasy, J. B. *Cell Cycle* **2004**, *3*, 998.
(7) Iwanaga, A.; Ouchida, M.; Miyazaki, K.; Hori, K.; Mukai, T. *Mutat. Res., DNA Repair* **1999**, *435*, 121.
(8) Nicolay, N. H.; Helleday, T.; Sharma, R. A. *Curr. Mol. Pharmacol.* **2012**, *5*, 54.
(9) Kunkel, T. A. *J. Biol. Chem.* **2004**, *279*, 16895.
(10) Seeberg, E.; Eide, L.; Bjoras, M. *Trends Biochem. Sci.* **1995**, *20*, 391.
(11) Friedberg, E. C. *Nature* **2003**, *421*, 436.
(12) Matsumoto, Y.; Kim, K. *Science* **1995**, *269*, 699.
(13) Maynard, S.; Schurman, S. H.; Harboe, C.; de Souza-Pinto, N. C.; Bohr, V. A. *Carcinogenesis* **2009**, *30*, 2.
(14) Loeb, L. A.; Monnat, R. J. *Nat. Rev. Genet.* **2008**, *9*, 594.
(15) Joyce, C. M.; Steitz, T. A. *Annu. Rev. Biochem.* **1994**, *63*, 777.
(16) Sawaya, M. R.; Prasad, R.; Wilson, S. H.; Kraut, J.; Pelletier, H. *Biochemistry* **1997**, *36*, 11205.
(17) Sawaya, M. R.; Pelletier, H.; Kumar, A.; Wilson, S. H.; Kraut, J. *Science* **1994**, *264*, 1930.
(18) Pelletier, H.; Sawaya, M. R.; Kumar, A.; Wilson, S. H.; Kraut, J. *Science* **1994**, *264*, 1891.
(19) Werneburg, B. G.; Ahn, J.; Zhong, X.; Hondal, R. J.; Kraynov, V. S.; Tsai, M. D. *Biochemistry* **1996**, *35*, 7041.
(20) Vande Berg, B. J.; Beard, W. A.; Wilson, S. H. *J. Biol. Chem.* **2001**, *276*, 3408.
(21) Arora, K.; Schlick, T. *Biophys. J.* **2004**, *87*, 3088.
(22) Arora, K.; Schlick, T. *J. Phys. Chem. B* **2005**, *109*, 5358.
(23) Kraynov, V. S.; Werneburg, B. G.; Zhong, X.; Lee, H.; Ahn, J.; Tsai, M. D. *Biochem. J.* **1997**, *323*, 103.
(24) Yang, L.; Beard, W. A.; Wilson, S. H.; Broyde, S.; Schlick, T. *J. Mol. Biol.* **2002**, *317*, 651.
(25) Radhakrishnan, R.; Schlick, T. *Proc. Natl. Acad. Sci. U.S.A.* **2004**, *101*, 5970.
(26) Beard, W. A.; Osheroff, W. P.; Prasad, R.; Sawaya, M. R.; Jaju, M.; Wood, T. G.; Kraut, J.; Kunkel, T. A.; Wilson, S. H. *J. Biol. Chem.* **1996**, *271*, 12141.
(27) Yang, L. J.; Beard, W. A.; Wilson, S. H.; Broyde, S.; Schlick, T. *Biophys. J.* **2004**, *86*, 3392.
(28) Yang, L.; Arora, K.; Beard, W. A.; Wilson, S. H.; Schlick, T. *J. Am. Chem. Soc.* **2004**, *126*, 8441.
(29) Radhakrishnan, R.; Schlick, T. *Biochem. Biophys. Res. Commun.* **2006**, *350*, 521.
(30) Nagel, Z. D.; Klinman, J. P. *Chem. Rev.* **2010**, *110*, PR41.
(31) Lin, P.; Batra, V. K.; Pedersen, L. C.; Beard, W. A.; Wilson, S. H.; Pedersen, L. G. *Proc. Natl. Acad. Sci. U.S.A.* **2008**, *105*, 5670.
(32) Schlick, T.; Collepardo-Guevara, R.; Halvorsen, L. A.; Jung, S.; Xiao, X. *Q. Rev. Biophys.* **2011**, *44*, 191.
(33) Beard, W. A.; Wilson, S. H. *Structure* **2003**, *11*, 489.
(34) Santoso, Y.; Joyce, C. M.; Potapova, O.; Le Reste, L.; Hohlbein, J.; Torella, J. P.; Grindley, N. D. F.; Kapanidis, A. N. *Proc. Natl. Acad. Sci. U.S.A.* **2010**, *107*, 715.
(35) Johnson, K. A. *J. Biol. Chem.* **2008**, *283*, 26297.
(36) Kellinger, M. W.; Johnson, K. A. *Proc. Natl. Acad. Sci. U.S.A.* **2010**, *107*, 7734.
(37) Tsai, Y. C.; Johnson, K. A. *Biochemistry* **2006**, *45*, 9675.
(38) Nashine, V. C.; Hammes-Schiffer, S.; Benkovic, S. J. *Curr. Opin. Chem. Biol.* **2010**, *14*, 644.
(39) Karplus, M. *Proc. Natl. Acad. Sci. U.S.A.* **2010**, *107*, E71.
(40) Prasad, B. R.; Warshel, A. *Proteins: Struct., Funct., Bioinf.* **2011**, *79*, 2900.
(41) Kamerlin, S. C. L.; Warshel, A. *Proteins: Struct., Funct., Bioinf.* **2010**, *78*, 1339.
(42) Ram Prasad, B.; Warshel, A. *Proteins* **2011**, *79*, 2900.
(43) MacKerell, A. D.; Bashford, D.; Bellott, M.; Dunbrack, R. L.; Evanseck, J. D.; Field, M. J.; Fischer, S.; Gao, J.; Guo, H.; Ha, S.; Joseph-McCarthy, D.; Kuchnir, L.; Kuczera, K.; Lau, F. T. K.; Mattos, C.; Michnick, S.; Ngo, T.; Nguyen, D. T.; Prodhom, B.; Reiher, W. E.; Roux, B.; Schlenkrich, M.; Smith, J. C.; Stote, R.; Straub, J.; Watanabe, M.; Wiorkiewicz-Kuczera, J.; Yin, D.; Karplus, M. *J. Phys. Chem. B* **1998**, *102*, 3586.
(44) MacKerell, A. D.; Banavali, N. K. *J. Comput. Chem.* **2000**, *21*, 105.
(45) Mackerell, A. D., Jr.; Feig, M.; Brooks, C. L., III. *J. Comput. Chem.* **2004**, *25*, 1400.
(46) Dellago, C.; Bolhuis, P. G.; Chandler, D. *J. Chem. Phys.* **1998**, *108*, 9236.
(47) Bolhuis, P. G.; Dellago, C.; Chandler, D. *Faraday Discuss.* **1998**, *110*, 421.
(48) Bolhuis, P. G.; Dellago, C.; Chandler, D. *Proc. Natl. Acad. Sci. U.S.A.* **2000**, *97*, 5877.
(49) Marti, J.; Csajka, F. S. *Phys. Rev. E* **2004**, *69*, 061918.
(50) Hagan, M. F.; Dinner, A. R.; Chandler, D.; Chakraborty, A. K. *Proc. Natl. Acad. Sci. U.S.A.* **2003**, *100*, 13922.
(51) Marti, J. *J. Phys.: Condens. Matter* **2004**, *16*, 5669.
(52) Bolhuis, P. G. *Proc. Natl. Acad. Sci. U.S.A.* **2003**, *100*, 12129.
(53) Juraszek, J.; Bolhuis, P. G. *Proc. Natl. Acad. Sci. U.S.A.* **2006**, *103*, 15859.
(54) Evans, D. A.; Wales, D. J. *J. Chem. Phys.* **2004**, *121*, 1080.
(55) Radhakrishnan, R.; Schlick, T. *J. Am. Chem. Soc.* **2005**, *127*, 13245.
(56) Wang, Y. L.; Schlick, T. *BMC Struct. Biol.* **2007**, *7*.
(57) Quaytman, S. L.; Schwartz, S. D. *Proc. Natl. Acad. Sci. U.S.A.* **2007**, *104*, 12253.
(58) Basner, J. E.; Schwartz, S. D. *J. Am. Chem. Soc.* **2005**, *127*, 13822.
(59) Saen-oon, S.; Quaytman-Machleder, S.; Schramm, V. L.; Schwartz, S. D. *Proc. Natl. Acad. Sci. U.S.A.* **2008**, *105*, 16543.
(60) Shah, A. M.; Li, S. X.; Anderson, K. S.; Sweasy, J. B. *J. Biol. Chem.* **2001**, *276*, 10824.
(61) Kosa, J. L.; Sweasy, J. B. *J. Biol. Chem.* **1999**, *274*, 3851.
(62) Joyce, C. M.; Grindley, N. D. F. *Proc. Natl. Acad. Sci.* **1983**, *80*, 1830.
(63) Derbyshire, V.; Grindley, N. D. F.; Joyce, C. M. *EMBO J.* **1991**, *10*, 17.
(64) Otwinowski, Z.; Minor, W. *Methods Enzymol.* **1997**, *276*, 307.
(65) Adams, P. D.; Afonine, P. V.; Bunkoczi, G.; Chen, V. B.; Davis, I. W.; Echols, N.; Headd, J. J.; Hung, L.-W.; Kapral, G. J.; Grosse-Kunstleve, R. W.; McCoy, A. J.; Moriarty, N. W.; Oeffner, R.; Read, R. J.; Richardson, D. C.; Richardson, J. S.; Terwilliger, T. C.; Zwart, P. H. *Acta Crystallogr.* **2010**, *D66*, 213.
(66) Emsley, P.; Lohkamp, B.; Scott, W. G.; Cowtan, K. *Acta Crystallogr.* **2010**, *D66*, 486.
(67) Davis, I. W.; Leaver-Fay, A.; Chen, V. B.; Block, J. N.; Kapral, G. J.; Wang, X.; Murray, L. W.; Arendall, W. B., III; Snoeyink, J.; Richardson, J. S.; Richardson, D. C. *Nucleic Acids Res.* **2007**, *35*, W375.
(68) DeLano, W. L. The PyMOL Molecular Graphics System, 2001.
(69) Brooks, B. R.; Bruccoleri, R. E.; Olafson, B. D.; States, D. J.; Swaminathan, S.; Karplus, M. *J. Comput. Chem.* **1983**, *4*, 187.

(70) Humphrey, W.; Dalke, A.; Schulten, K. *J. Mol. Graphics Modell.* **1996**, *14*, 33.
(71) Phillips, J. C.; Braun, R.; Wang, W.; Gumbart, J.; Tajkhorshid, E.; Villa, E.; Chipot, C.; Skeel, R. D.; Kale, L.; Schulten, K. *J. Comput. Chem.* **2005**, *26*, 1781.
(72) Feller, S. E.; Zhang, Y. H.; Pastor, R. W.; Brooks, B. R. *J. Chem. Phys.* **1995**, *103*, 4613.
(73) Darden, T.; York, D.; Pedersen, L. *J. Chem. Phys.* **1993**, *98*, 10089.
(74) Pratt, L. R. *J. Chem. Phys.* **1986**, *85*, 5045.
(75) Bolhuis, P. G.; Chandler, D.; Dellago, C.; Geissler, P. L. *Annu. Rev. Phys. Chem.* **2002**, *53*, 291.
(76) Radhakrishnan, R.; Schlick, T. *J. Chem. Phys.* **2004**, *121*, 2436.
(77) Kirby, T. W.; Derose, E. F.; Cavanaugh, N. A.; Beard, W. A.; Shock, D. D.; Mueller, G. A.; Wilson, S. H.; London, R. E. *Nucleic Acids Res.* **2012**, *40*, 2974.
(78) Kraynov, V. S.; Showalter, A. K.; Liu, J.; Zhong, X. J.; Tsai, M. D. *Biochemistry* **2000**, *39*, 16008.
(79) Arora, K.; Beard, W. A.; Wilson, S. H.; Schlick, T. *Biochemistry* **2005**, *44*, 13328.
(80) Ahn, J.; Werneburg, B. G.; Tsai, M. D. *Biochemistry* **1997**, *36*, 1100.
(81) Ahn, J. W.; Kraynov, V. S.; Zhong, X. J.; Werneburg, B. G.; Tsai, M. D. *Biochem. J.* **1998**, *331*, 79.
(82) Murphy, D. L.; Jaeger, J.; Sweasy, J. B. *J. Am. Chem. Soc.* **2011**, *133*, 6279.
(83) Yamtich, J.; Starcevic, D.; Lauper, J.; Smith, E.; Shi, I.; Rangarajan, S.; Jaeger, J.; Sweasy, J. B. *Biochemistry* **2010**, *49*, 2326.
(84) Murphy, D. L.; Kosa, J.; Jaeger, J.; Sweasy, J. B. *Biochemistry* **2008**, *47*, 8048.
(85) Dalal, S.; Hile, S.; Eckert, K. A.; Sun, K. W.; Starcevic, D.; Sweasy, J. B. *Biochemistry* **2005**, *44*, 15664.
(86) Dalal, S.; Kosa, J. L.; Sweasy, J. B. *J. Biol. Chem.* **2004**, *279*, 577.
(87) Kosa, J. L.; Sweasy, J. B. *J. Biol. Chem.* **1999**, *274*, 35866.
(88) Fiala, K. A.; Suo, Z. *Biochemistry* **2004**, *43*, 2116.
(89) Eger, B. T.; Benkovic, S. J. *Biochemistry* **1992**, *31*, 9227.
(90) Venkatramani, R.; Radhakrishnan, R. *Proteins: Struct., Funct., Bioinf.* **2008**, *71*, 1360.